Journal of Advanced Marine Engineering and Technology, Vol. 48, No. 5, pp. 277~286, 2024
J. Advanced Marine Engineering and Technology (JAMET)
https://doi.org/10.5916/jamet.2024.48.5.277

ISSN 2234-7925 (Print)
ISSN 2765-4796 (Online)
Original Paper

Kinetics Rate Characteristics of Reformate Gas in a Reformer for Hydrogen Production

Da-Hye Hwang[1] · Yong-Seok Choi[2] · Tae-Woo Lim[†]

(Received September 19, 2024 ; Revised October 13, 2024 ; Accepted October 29, 2024)

Abstract: The mechanism of a water–gas shift (WGS) reactor design was analyzed to produce hydrogen using part of the boil-off gas (BOG) generated from liquefied natural gas (LNG) used as fuel in propulsion ships, and to produce propulsion power for the ships by utilizing the produced hydrogen in fuel cells. Methane, which is the main component of LNG, can be used to produce hydrogen through a high-temperature steam–methane reforming (SMR) reaction. However, in the SMR reactor, carbon monoxide is generated as a by-product, which can cause catalyst poisoning, which in turn causes the shift reaction rate to decrease. To prevent the reforming reaction from being inhibited by carbon monoxide, the WGS reaction can be employed to convert it into carbon dioxide, which can then be collected using a carbon capture system device to prevent air pollution. In this study, the reaction results of SMR using methane as a fuel and the effect of process variables on the WGS reaction, such as temperature, pressure, and S/C ratio, were predicted using Microsoft Excel and MATLAB. The predictions focused on the methane and carbon monoxide conversions as functions of the lengths of the SMR and WGS reactors. In the WGS reactor, when the S/C ratio ranged from 2 to 6, the CO conversion increased as the S/C ratio decreased, but the conversion values differed by less than 4%. Furthermore, as the temperature decreased and the pressure increased, the CO conversion increased, and as the temperature and pressure increased, the required length of the WGS reactor decreased. However, the CO conversion that reached equilibrium increased as the temperature decreased and the pressure increased; therefore, increasing the pressure of the WGS reactor can achieve a high CO conversion rate with a short WGS reactor length. Based on these results, further research can be conducted to suitably design reactors for installation on maritime vessels.

Keywords: Boil-off gas, Fuel cell, Hydrogen production, Steam–methane reforming, Water–gas shift reaction

Nomenclature

c(CO)	concentration of CO, mol/m^3
c_{CO}(T)	inlet concentration of CO at T, mol/m^3
E	activation energy, kJ/kmol
k	rate constant, 1/s
k_0	pre-exponential factor
K_{eq}	equilibrium constant
M	water to carbon monoxide ratio
n_{CO}	inlet molar flow rate of CO, mol/h
L	catalyst bed length, m
P_{total}	Total pressure, kPa
p	partial pressure, bar
R_g	gas constant, =8.314 kJ/kmol
r	pipe inlet diameter, m
S	selectivity
T	temperature, K
V_{CO}	inlet volumetric flow rate, cm^3/s
V_{total}	total inlet volumetric flow rate, cm^3/s
W	conversion rate
X_{CO}	conversion of CO in WGS
Y	hydrogen yield
ρ	catalyst bulk density, g/cm^3

Subscripts

m	concentration exponent of H_2O
n	concentration exponent of CO
SMR	Steam Methane Reformer
WGS	Water Gas Shift

† Corresponding Author (ORCID: http://orcid.org/0000-0002-3925-0731): Professor, Division of Marine Engineering, Korea Maritime & Ocean University, 727, Taejong-ro, Yeongdo-gu, Busan 49112, Korea, E-mail: kyunlim@kmou.ac.kr, Tel: +82-51-410-4256

1 Ph. D. Candidate, Graduate school of Korea Maritime & Ocean University, E-mail: dahye@g.kmou.ac.kr

2 Professor, Division of Coast Guard Studies, Korea Maritime &Ocean University, E-mail: choiys@kmou.ac.kr

WGSR Water Gas Shift Reaction

1. Introduction

As the effects of global climate change intensify, achieving zero carbon emissions has become an important goal for modern society **[1]**. At the 80th meeting of the International Maritime Organization's Maritime Environment Protection Committee (MEPC) in London, England in July 2023, targets were set for decarbonization and reduction of greenhouse gas (GHG) emissions from maritime vessels **[2]**. To achieve the goal set for 2050, member states have agreed on the need to form a framework for intermediate measures to accelerate the energy transition in the shipping industry; to this end, it is necessary to establish sequential goals and respond to changes in the environmental regulatory paradigm, such as by expanding eco-friendly vantage and using decarbonized fuels **[2]**.

International transport is essential to world trade, so much so that 80% of global trade in 2018 was carried out via maritime transportation **[3]**. Therefore, the task of implementing decarbonization in the shipping industry is becoming more crucial. Using low-carbon and zero-carbon fuels is the most effective strategy to reduce emissions from maritime vessels; however, it is very difficult to realize this immediately because of constraints such as vessel type, shipping route, demand, alternative fuels, policy, and lack of technology **[4]**. To achieve decarbonization in the global energy market in the future, the deployment of commercially available technologies and accessibility to low-carbon fuels are crucial; therefore, prior research on the requirements for a zero-carbon society is essential **[5]**.

Hydrogen is a clean and renewable energy source with a high energy density and does not produce harmful emissions upon combustion; therefore, it can be considered the most effective fuel for minimizing environmental problems **[6]**. By generating power using hydrogen, benefits such as reduced greenhouse effect, reduced use of fossil fuels, expansion of renewable energy for energy storage, and reduced environmental pollution can be achieved **[7]**. Hydrogen can be produced through three main processes involving the reforming of hydrocarbon molecules from natural gas, which is a readily available fossil fuel **[8]**. Today, nearly 98% of hydrogen (96% in 2018) originates from fossil fuel sources via steam methane reforming (SMR) (76%) or coal gasification (22%). Only 2% of the hydrogen is produced from renewable sources, mainly through water splitting **[9]**.

Considering the environmental impact of the production method used, hydrogen can be classified as gray, blue, or green hydrogen **[10]**. Gray hydrogen is produced from fossil fuels, and the process emits large amounts of CO_2 emissions. Blue hydrogen is produced in the same manner as gray hydrogen but involves reducing greenhouse gas emissions by capturing, compressing, and storing or recycling the CO_2 generated from the reforming reactions to prevent it from being released into the atmosphere. Green hydrogen is produced through water electrolysis; it is considered the most environmentally friendly hydrogen production method as it does not emit CO_2 and produces hydrogen and oxygen using electricity obtained from renewable energy sources such as hydropower, wind power, and solar power **[11][12]**. Owing to the high cost of green hydrogen, the production of blue hydrogen is considered an intermediate solution for transitioning to a hydrogen-based economy **[13]**. The methods for producing blue hydrogen include SMR, autothermal reforming, partial methane oxidation, and methane pyrolysis. SMR is the most widely used method, and simultaneous application of carbon capture technology can enable the production of low-carbon hydrogen from fossil fuels **[14]**.

Ali and Abdullah **[15]** analyzed the thermodynamic performance of a reforming process involving SMR and WGS reaction for producing hydrogen from LNG using solar energy as a renewable energy source with the aim of minimizing the environmental impact. The results of this study emphasize the importance of the operating temperature for both the SMR and WGS reactions, with the energy efficiency decreasing with increasing temperature. Therefore, while higher reforming temperatures resulted in more hydrogen production, the maximum operating temperature was limited to 850°C. Furthermore, the performance of the SMR reactor significantly influenced the overall system performance. Huang and Jhao **[16]** tested a series of samaria-doped ceria (SDC)/Ni-Cu catalysts for SMR. The introduction of Cu into Ni significantly enhances WGS activity in the presence of CO_2, while concurrently reducing the rate of CO production. These productions were found to be quantitatively correlated with the proportion of Cu-Ni species present. Kumar et al. **[17]** presented simulation models for SMR and steam biogas reforming (SBR) processes to produce eco-friendly hydrogen gas and minimize the burden of fossil fuels. Yusuf *et al.* **[18]** demonstrated efficient hydrogen production from boil-off gas (BOG)

generated in an onshore LNG facility through technical and socioeconomic analyses.

For convenience of transportation on vessels that run on LNG, the LNG fuel is maintained at cryogenic temperatures of approximately –163°C or lower at normal pressure. However, poor insulation of the cargo hold results in approximately 0.15% of the total fuel evaporating as BOG per day. As the LNG vaporizes due to heat loss, the volume in the tank increases, resulting in the tank pressure rapidly increasing. Therefore, for safety, it is necessary to maintain constant pressure in the tank **[19]**. One way to do so is to remove the BOG from the tank. **Figure 1** shows methods for treating the BOG generated in an LNG cargo hold: it can be used as fuel for ship propulsion engines, re-liquified, released into the atmosphere, or burned **[20]**. An additional method of performing SMR to convert it into hydrogen, which can then be used in fuel cells, has been proposed.

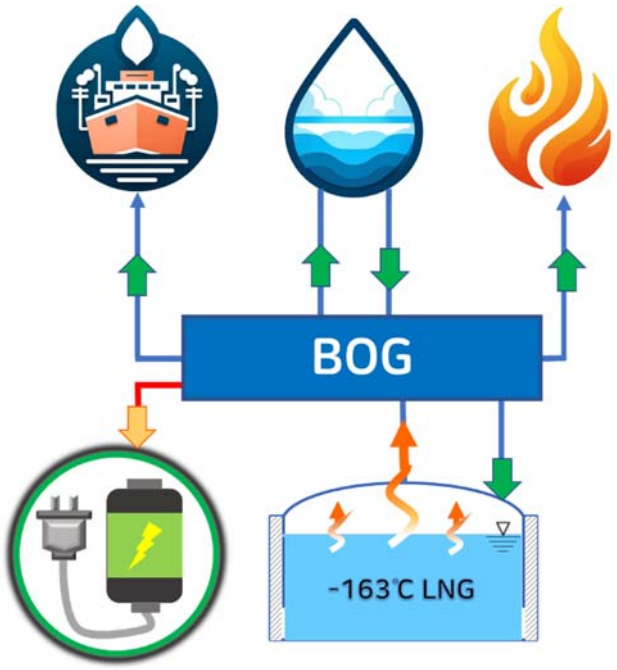

Figure 1: Treatment of boil-off gas (BOG) generated in LNG cargo holds owing to poor insulation

In this study, a continuous reaction to be performed in SMR and WGS reactors was designed using methane, the main component of BOG generated from vessels, as the feed gas. To reduce catalyst poisoning due to efficient hydrogen reduction and CO production and to design an optimal WGS reactor, the WGS reaction mechanism was analyzed by changing variables such as the reactor temperatures and pressures and the S/C ratio.

2. Hydrogen production methods

Figure 2: Types of hydrogen according to production method

Figure 2 shows the types of hydrogen depending on the hydrogen production method. Gray hydrogen, which is produced from fossil fuels, is produced through a catalytic chemical reaction between methane, the main component of natural gas, and high-temperature water vapor; this process emits CO_2 **[21]**.

Blue hydrogen is produced in the same manner as gray hydrogen; however, the process includes the carbon capture system (CCS) technology, which captures and stores the generated CO_2 rather than releasing it into the atmosphere, such as what occurs when producing gray hydrogen. It is therefore highly environmentally friendly, as less CO_2 is emitted than in gray hydrogen production. Furthermore, the CCS technology is highly mature and competitive. Therefore, blue hydrogen production is attracting attention as the most realistic alternative for decarbonization.

Green hydrogen is obtained by electrolyzing water, which produces hydrogen and oxygen. The electrical energy required for this process is obtained from renewable energy sources such as solar, wind, and hydro power. Therefore, it can be considered the most environmentally friendly form of hydrogen because there are no CO_2 emissions during the production process.

3. Process Description

3.1 Proposed Process

Figure 3 shows a conceptual schematic diagram for obtaining auxiliary power using hydrogen produced through an reactor in which both SMR and WGS are conducted in tandem using a fuel cell.

Part of the BOG generated in the LNG cargo hold is introduced into the SMR reactor at a high temperature along with steam to undergo SMR and WGS; the products are then introduced into

the WGS reactor at a low temperature to reduce the CO concentration and produce additional hydrogen.

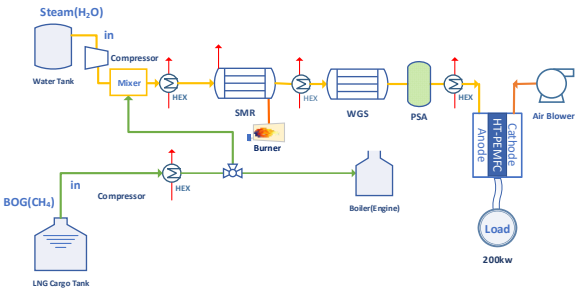

Figure 3: Schematic diagram of the proposed steam–methane reforming (SMR) process

The CO_2 generated from the SMR&WGS process is captured using pressure swing adsorption (PSA); therefore, the produced hydrogen can be classified as blue hydrogen. The additional power required by the maritime vessels can be obtained from fuel cells.

3.2 SMR and WGS Process

In SMR, hydrogen is produced through an endothermic reaction between methane and steam at high temperatures in the presence of a catalyst, as shown in **Equation (1)**; CO and a relatively small amount of CO_2 are also produced.

r_1: Steam–Methane Reforming Reaction

$$CH_4 + H_2O \Leftrightarrow CO + 3H_2, \Delta H = 206.1kJ/mol \quad (1)$$

If an exothermic water–gas conversion process is adopted in conjunction, SMR always produces CO_2 and hydrogen; this can increase the hydrogen yield. This conversion process, the WGS reaction, is shown in **Equation (2)**.

r_2: WGS Reaction

$$CO + H_2O \Leftrightarrow CO_2 + H_2, \Delta H = -41.15kJ/mol \quad (2)$$

Assuming that the auxiliary power to be obtained through SMR is 200 kW, the amount of CH_4 required is estimated to be 1.77 kmol/h. Using these values, an analysis was conducted for reducing CO catalyst poisoning and increasing hydrogen production through changes in the S/C ratio, temperature, and pressure of the SMR and WGS reactor.

One of the most important and economical methods for hydrogen production is the WGS reaction. However, because the conversion rate of the WGS reaction, which is a low-temperature exothermic reaction, decreases when performed along with the high-temperature SMR reaction, a separate low-temperature WGS reactor must be additionally installed. This can further facilitate the WGS reaction, thus reducing the CO concentration and consequently producing additional hydrogen.

The final reaction equation for the SMR reaction is shown in **Equation (3)**.

r_3: Direct Steam Reforming Reaction

$$CH_4 + 2H_2O \Leftrightarrow CO_2 + 4H_2, \Delta H = 164.9kJ/mol \quad (3)$$

3.3 Numerical Model

The model proposed by Keiski *et al.* **[22]** for estimating the change in the WGS reaction conversion rate along the length of the WGS reactor is shown in **Equation (4)-(7)**.

$$dX_{CO}/dL = (\rho\pi r^2/n_{CO})k_0 exp(-E/R_gT)$$
$$c_{CO}^{n+m}(1-X_{CO})^n(M-X_{CO})^m$$
$$\{1 - X_{CO}^2/[K_{eq}(1-X_{CO})(M-X_{CO})]\} \quad (4)$$

Where $c_{CO}(T) = (V_{CO}/V_{total})(P/R_gT)$ (5)

$n_{CO} = V_{total}c_{co}$ (at 293K) (6)

$K_{eq} = exp(4577.8/T - 4.33)$ (7)

Table 1: Initial conditions for the SMR and WGS process

Parameter	Value
CH_4 molar flow rate [kmol/h]	1.77
Steam Carbon ratio	2~6
SMR Temperature [℃]	600~900
WGS Temperature [℃]	160~250
Pressure [bar]	1~30
SMR tube O.D[m]	0.0217
SMR tube thickness[m]	0.0025
SMR tube number	10
WGS tube O.D[m]	0.0272
WGS tube thickness[m]	0.0025
WGS tube number	50

X_{CO} represents the CO conversion rate in the WGS reactor, L is the length of the WGS reactor, ρ is the bulk density of the catalyst, r is the pipe inlet diameter, n_{CO} is the inlet molar flow rate of CO, k_0 is the pre-exponential factor, k_{eq} is the equilibrium

constant, E is the activation energy, R_g is the gas constant, c_{CO} is the concentration of CO, V_{CO} is the inlet volumetric flow rate of CO, and V_{total} is the total inlet volumetric flow rate. In addition, to determine the index value, it was assumed that the ICI–CuZnO/Al_2O_3 catalyst was used. Parameters for the process design are shown in **Table 1**.

4. Results and Discussion

Figure 4 shows the change in CH_4 conversion and S/C ratio according to the SMR reactor length when the SMR pressure and temperature are 3 bar 750°C, respectively. CH_4 converted rapidly within a SMR reactor length of 0.1 m. At S/C ratios of 2 and 6, the equilibrium conversion was 0.85 and 0.82, respectively; therefore, the difference in CH_4 conversion due to an increase in the S/C ratio was less than 3%. Note that while the CH_4 conversion rate increased with increasing S/C ratio, the speed of CH_4 conversion became slower. The SMR reactor length required for the CH_4 conversion rate to reach an equilibrium state was 0.607 m when the S/C ratio was 2 and 1.477 m when the S/C ratio was 6; the reactor length required to achieve equilibrium increased by approximately 2.43 times.

Figure 5 shows the CO conversion according to the WGS reactor length and S/C ratio when the pressure of the SMR reactor was 3 bar and the temperatures of the SMR and WGS reactors were 750°C and 160°C, respectively. CO converted rapidly within a WGS reactor length of 0.3 m. At S/C ratios of 2 and 6, the CO conversion was 0.735 and 0.695, respectively; that is, the difference in CO conversion owing to the increase in S/C ratio was less than 4%. Regardless of the S/C ratio increasing or decreasing, there was little difference in the CO conversion rate reaching equilibrium or the WGS reactor length.

Figure 6 shows the CH_4 conversion according to the SMR reactor length and temperature when the SMR pressure was 3 bar and the S/C ratio was 3. CH_4 conversion underwent a sharp increase within a SMR reactor length of 0.1 m. As the temperature was increased from 600°C to 900°C, the CH_4 conversion increased significantly from 0.1 to 0.96. Therefore, as the temperature increased, not only did the rate of CH_4 conversion accelerate, but high CH_4 conversion could be obtained. For the CH_4 conversion to reach equilibrium, the length of the SMR reactor had to be decreased with increasing temperature, from 0.937 m at 600°C to 0.182 m at 900°C.

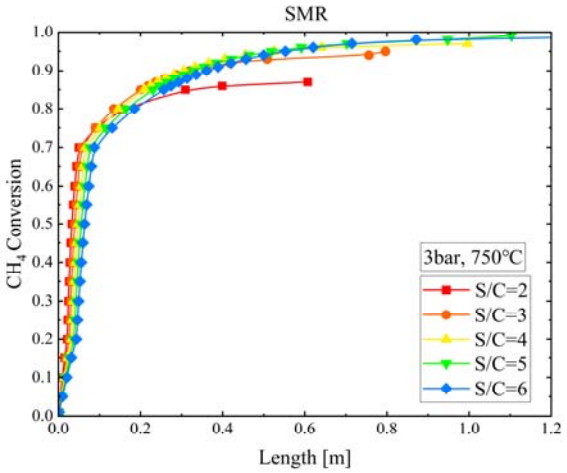

Figure 4: CH_4 conversion at the SMR reactor outlet according to the SMR reactor length and S/C ratio

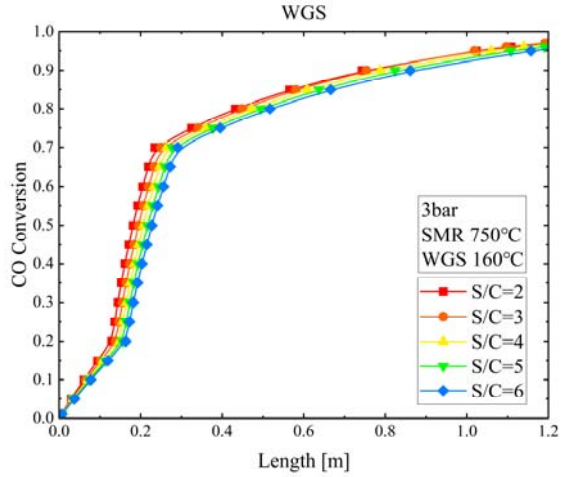

Figure 5: CH_4 conversion at the water–gas shift (WGS) reactor outlet according to the WGS reactor length and S/C ratio

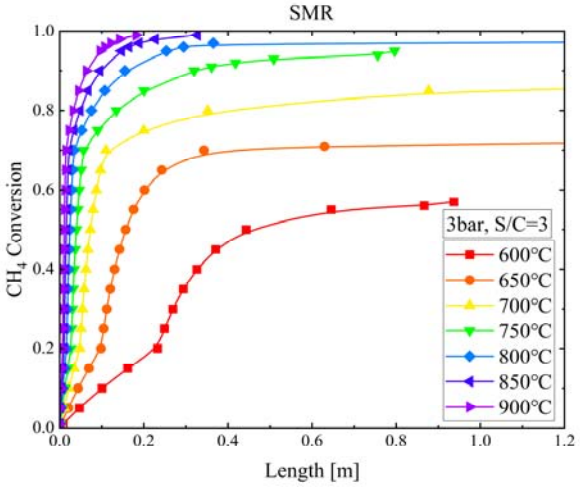

Figure 6: CH_4 conversion at the SMR reactor outlet according to the SMR reactor length and temperature

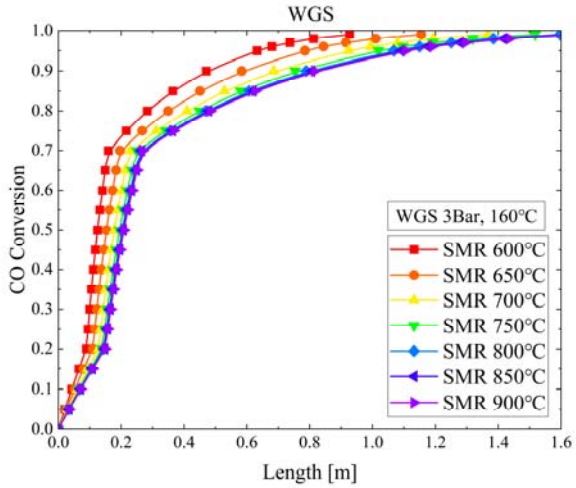

Figure 7: CO conversion at the WGS reactor outlet according to the WGS reactor length and SMR temperature

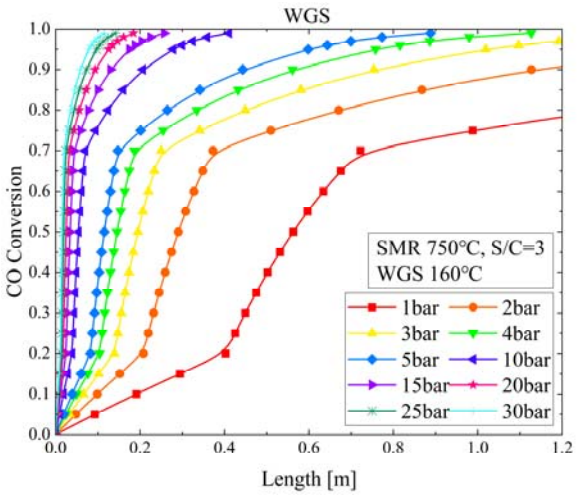

Figure 10: CO conversion at the WGS reactor outlet according to the WGS reactor length and pressure

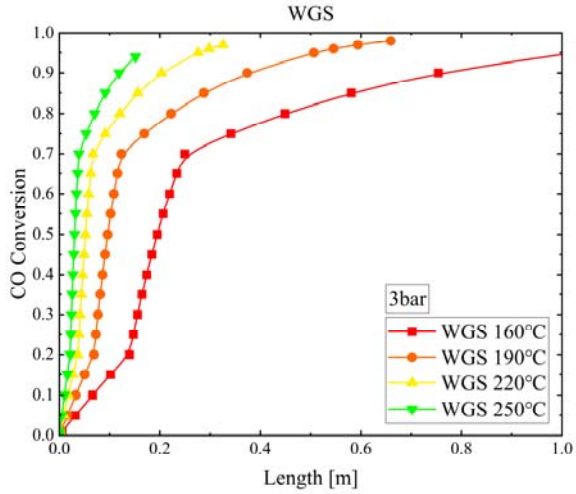

Figure 8: CO conversion at the WGS reactor outlet according to the WGS reactor length and temperature

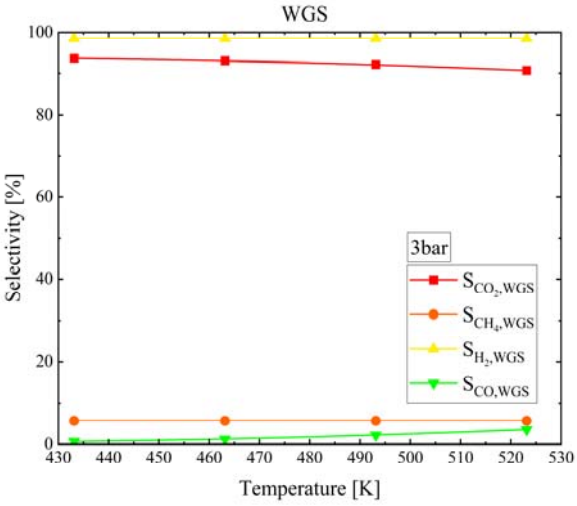

Figure 11: Selectivities for CH_4, CO, CO_2, and H_2 at the WGS reactor outlet according to the WGS temperature

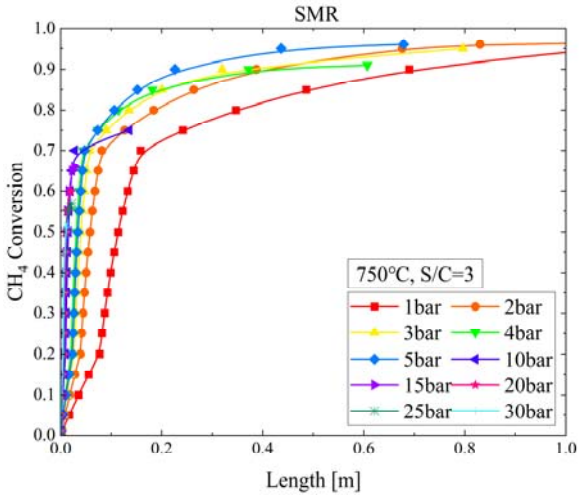

Figure 9: CH_4 conversion at the SMR reactor outlet according to the SMR reactor length and pressure

Figure 7 shows the CO conversion according to the WGS reactor length and SMR temperature when the WGS pressure and temperature were 3 bar and 160°C, respectively. CO rapidly converted within a WGS reactor length of 0.3 m. When the SMR temperature was increased from 600°C to 900°C, the CO conversion decreased from 0.81 to 0.715; that is, when the SMR temperature was increased by 300°C, the CO conversion decreased by approximately 10%. Furthermore, with this increase in SMR temperature, the length of the WGS reactor increased by approximately 1.8 times, from 0.93 m to 1.66 m.

Figure 8 shows the CO conversion rate according to the WGS reactor length and WGS temperature when the pressure of the WGS reactor was 3 bar. CO rapidly converted at the beginning

of the reaction. As the WGS temperature increased, the CO conversion at which the WGS reaction reached equilibrium decreased. Furthermore, with an increase in WGS temperature from 160°C to 250°C, the WGS reactor length required to reach equilibrium significantly decreased from 1.51 m to 0.15 m.

Figure 9 shows the CH_4 conversion according to the SMR reactor length and pressure change when the SMR temperature was 750°C and S/C ratio was 3. As the pressure increased, the final CH_4 conversion decreased, and the SMR reactor length required to reach the reforming equilibrium state decreased from 2.56 m at 1 bar to 1.43 m at 2 bar, 0.8 m at 3 bar, 0.68 m at 5 bar, and 0.013 m at 30 bar.

Figure 10 shows the CO conversion according to the WGS reactor length and pressure change when the SMR temperature was 750°C, S/C ratio was 3, and WGS temperature was 160°C. As the pressure increased from 1 to 30 bar, the CO conversion at which the WGS reaction reached equilibrium decreased by 53% from 0.99 to 0.52. Additionally, as the pressure increased, the WGS reactor length required to reach equilibrium decreased from 4.4259 m at 1 bar to 1.12 m at 4 bar, 0.41 m at 10 bar, and 0.11 m at 30 bar.

Figure 11 shows the selectivities for CH_4, CO, CO_2, and H_2 (S_{CH_4}, S_{CO}, S_{CO_2}, and S_{H_2}, respectively) at the WGS reactor outlet with respect to the WGS temperature at a pressure of 3 bar. As the temperature increased from 160°C to 250°C, S_{CH_4} remained unchanged at 5.72%, S_{CO} increased from 0.61% to 3.55%, S_{CO_2} decreased from 93.7% to 90.7%, and S_{H_2} exhibited almost no change at 98.5%.

Figure 12 shows the S_{CH_4}, S_{CO}, S_{CO_2}, and S_{H_2} values at the WGS reactor outlet based on the SMR&WGS pressure when the pressure was 3 bar. As the pressure increased, S_{CH_4} increased from 0.79% to 47.23%, S_{CO} from 0.74% to 0.11%, S_{CO_2} from 98.5% to 52.65%, and S_{H_2} from 99.8% to 81.7%.

Figure 13 shows the S_{CH_4}, S_{CO}, S_{CO_2}, and S_{H_2} values at the WGS reactor outlet according to the S/C ratio at a pressure of 3 bar. As the S/C ratio increased, S_{CH_4} decreased from 13.1% to 0.88%, S_{CO} decreased from 2.03% to 0.19%, S_{CO_2} decreased from 84.9% to 98.9%, and S_{H_2} increased from 96.4% to 99.8%.

Figure 14 shows the hydrogen yields at the SMR and WGS reactor outlets ($Y_{H_{2,SMR}}$ and $Y_{H_{2,WGS}}$, respectively) according to the S/C ratio when the pressure was 3 bar, SMR temperature was 750°C, and WGS temperature was 160°C. As the S/C ratio increased, the $Y_{H_{2,SMR}}$ increased from 35.9% to 45.0% and the $Y_{H_{2,WGS}}$ increased from 43.4% to 49.8%.

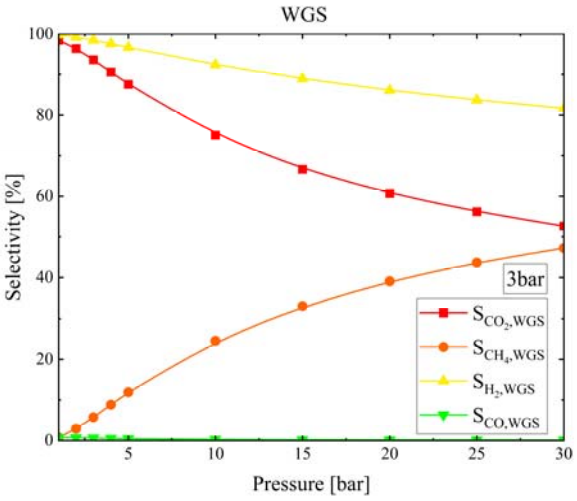

Figure 12: Selectivities for CH_4, CO, CO_2, and H_2 at the WGS reactor outlet according to the pressure

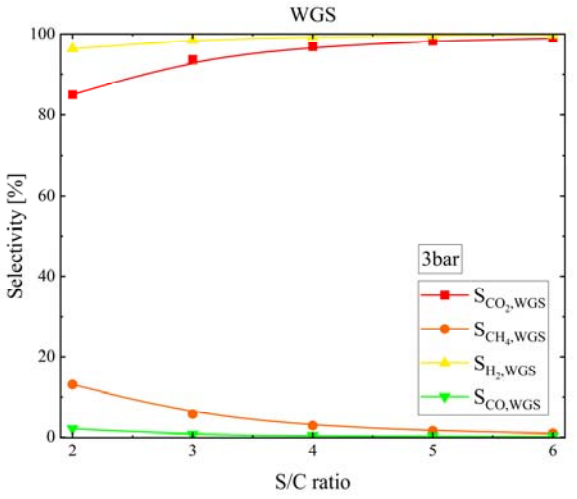

Figure 13: Selectivities for CH_4, CO, CO_2, and H_2 at the WGS reactor outlet according to the S/C ratio

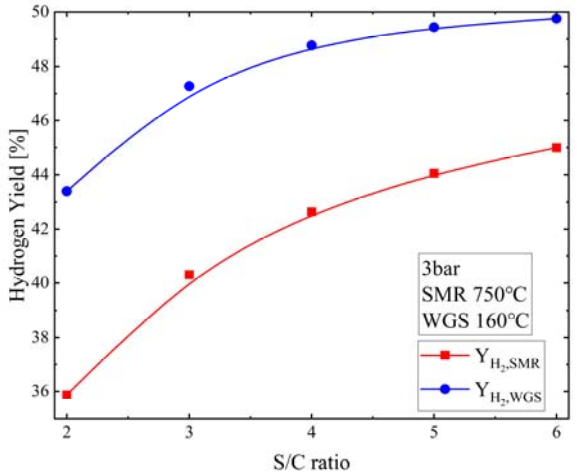

Figure 14: Hydrogen yields at the SMR and WGS reactor outlets according to the S/C ratio

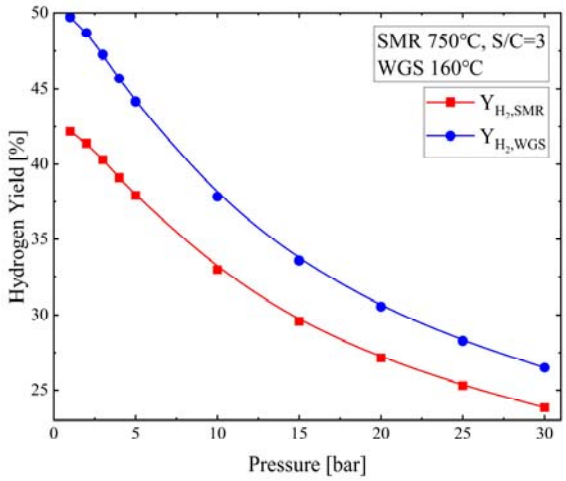

Figure 15: Hydrogen yields at the SMR and WGS reactor outlets according to pressure

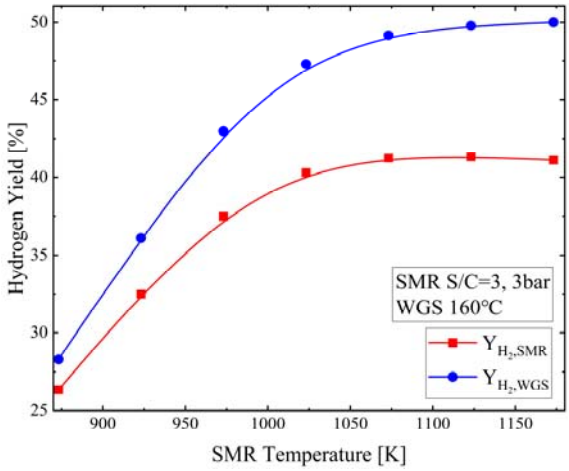

Figure 16: Hydrogen yield at the WGS reactor outlet according to the SMR temperature.

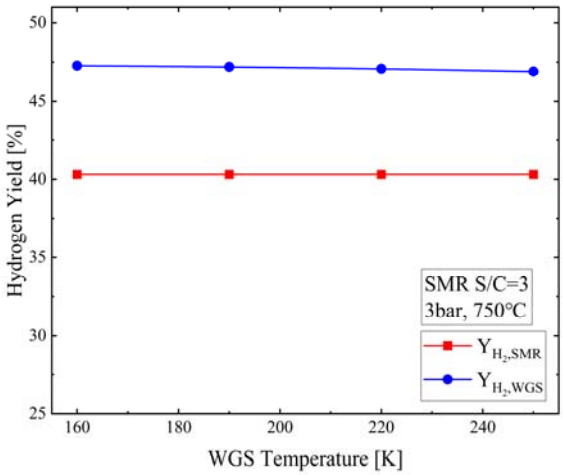

Figure 17: Hydrogen yield at the WGS reactor outlet according to the WGS temperature.

Figure 15 shows the $Y_{H_{2,SMR}}$ and $Y_{H_{2,WGS}}$ according to pressure when the S/C ratio was 3, SMR temperature was 750°C, and WGS temperature was 160°C. As the pressure increased, the $Y_{H_{2,SMR}}$ decreased from 42.2% to 23.8% and the $Y_{H_{2,WGS}}$ decreased from 49.7% to 26.5%.

Figure 16 shows the $Y_{H_{2,SMR}}$ and $Y_{H_{2,WGS}}$ according to the SMR temperature when the S/C ratio was 3, SMR pressure and temperature were 3 bar and 750°C, respectively, and WGS temperature was 160°C. As the SMR temperature increased , the $Y_{H_{2,SMR}}$ increased from 26.4% to 41.3%, though it decreased slightly to 41.1%, while the $Y_{H_{2,WGS}}$ increased from 28.3% to 50.0%.

Figure 17 shows the $Y_{H_{2,SMR}}$ and $Y_{H_{2,WGS}}$ at the WGS reactor outlet according to the WGS temperature when the S/C ratio was 3 and the SMR pressure and temperature were 3 bar and 750°C, respectively. As the WGS temperature increased, $Y_{H_{2,SMR}}$ did not change and remained at 40.3%, while $Y_{H_{2,WGS}}$ decreased from 47.3% to 46.9%.

5. Conclusion

1. As the S/C ratio and SMR temperature increased, the CH_4 conversion in the SMR reactor increased. In contrast, in the WGS reactor, as the S/C ratio decreased, the CO conversion increased; however, when the S/C ratio was in the range 2–6, the CO conversion changed by less than 4%. Meanwhile, as the temperature decreased and pressure increased in the WGS reactor, the CO conversion increased.
2. As the pressure in the SMR reactor increased, the CH_4 conversion decreased; however, the SMR reactor length required to reach equilibrium conversion decreased. In the WGS reactor, as the pressure increased, the CO conversion increased, and the WGS reactor length required for the WGS reaction decreased.
3. Compared with the increase in CH_4 conversion with the SMR temperature, the change in CO conversion with the WGS temperature was not significant.
4. The simultaneous SMR and WGS process in the SMR reactor exhibited a high CO conversion at the SMR reactor inlet regardless of the reaction temperature or pressure.
5. The S_{CO}, S_{CO_2}, S_{H_2}, and S_{CH_4} values at the WGS reactor outlet changed by less than 5% with changing temperature. As the WGS temperature increased, the equilibrium CO conversion decreased, but the CO conversion rate increased rapidly near

the WGS reactor inlet; therefore, the required length of the WGS reactor decreased. Additionally, as the pressure increased, S_{CO}, S_{CO_2}, and S_{H_2} decreased, but the reaction period was short. Therefore, the WGS reactor length could be designed to be short.

6. As the pressure at the WGS reactor outlet increased, the hydrogen yield ($Y_{H_{2,WGS}}$) decreased, but was still larger than that at the SMR reactor outlet ($Y_{H_{2,SMR}}$).

Based on the above findings, we plan to continue our research to size the WGS reactor such that it can be installed on maritime vessels and design the optimal operating point depending on the effects of changes in the temperature, pressure, and S/C ratio of the SMR and WGS reactors.

Author Contributions

Conceptualization, D. H. Hwang; Methodology, D. H. Hwang; Software, D. H. Hwang; Formal Analysis, D. H. Hwang; Investigation, Y. S. Choi; Resources, T.W.Lim; Data Curation D. H. Hwang; Writing-Original Draft Preparation, D. H. Hwang; Writing-Review & Editing, T.W.Lim; Visualization, Y. S. Choi; Supervision, T.W.Lim;

References

[1] N. Slawinski and P. Bansal, "A matter of time: The temporal perspectives of organizational responses to climate change," Organization Studies, vol. 33, no. 11, 2012.

[2] MARITIME FORECAST TO 2050, Energy Transition Outlook DNV, 2024.

[3] S. N. Sirimanne, J. Hoffman, W. Juan, R. Asariotis, M. Assaf, G. Ayala, "Review of maritime transport," United Nations Conference on Trade And Development, Geneva, Switzerland, 2019

[4] Z. Wang, B. Dong, J. Yin, M. Li, Y. Ji, and F. Han, "Towards a marine green power system architecture: Integrating hydrogen and ammonia as zero-carbon fuels for sustainable shipping," International Journal of Hydrogen Energy, vol. 50, Part B, pp. 1069-1087, 2024.

[5] G. Di Foggia, M. Beccarello, "Decarbonization in the European steel industry: Strategies, risks, and commitments," Environmental Challenges, vol. 16, 100988, 2024.

[6] T. Khan, M. Yu, and M. Waseem, "Review on recent optimization strategies for hybrid renewable energy system with hydrogen technologies: State of the art, trends and future directions," International Journal of Hydrogen Energy, vol. 47, no. 60, pp. 25155-25201, 2022.

[7] A. Golmakani, S. Fatemi, and J. Tamnanloo, "Investigating PSA, VSA, and TSA methods in SMR unit of refineries for hydrogen production with fuel cell specification," Separation and Purification Technology," vol. 176, pp. 73-91, 2017.

[8] M. McBain, J. Hollingsworth, S. Freund, T. Allison, S. Harvey, *et al.*, "Chapter 7 - Transport of hydrogen and carriers of hydrogen," Energy Transport Infrastructure for a Decarbonized Economy, pp. 291-328, 2025

[9] T. Lepage, M. Kammoun, Q. Schmetz, and A. Richel, "Biomass-to-hydrogen: A review of main routes production, processes evaluation and techno-economical assessment," Biomass and Bioenergy, vol. 144, 105920, 2021.

[10] M. Noussan, P. P. Raimondi, R. Scita, and M. Hafner, "The role of green and blue hydrogen in the energy transition—a technological and geopolitical perspective," Sustainability, vol. 13, no. 1, 298, 2021.

[11] G. Kakoulaki, I. Kougias, N. Taylor, F. Dolci, J. Moya, A. Jäger-Waldau, "Green hydrogen in Europe – a regional assessment: substituting existing production with electrolysis powered by renewables," Energy Conversion and Management, vol. 228, 113649, 2021.

[12] R. G. Lemus and J. M. Martínez Duart, "Updated hydrogen production costs and parities for conventional and renewable technologies," International Journal of Hydrogen Energy, vol. 35, no. 9, pp. 3929-3936, 2010.

[13] D. Alghool, M. Haouari, and P. Trucco, "It is not the same blue: A comparative LCA study of blue hydrogen supply network pathways," International Journal of Hydrogen Energy, vol. 81, pp. 214-224, 2024.

[14] G. Brändle, M. Schönfisch, and S. Schulte, "Estimating long-term global supply costs for low-carbon hydrogen," Applied Energy, vol. 302, 117481, 2021.

[15] A. Alaidaros, A. A. AlZahrani, "Integrated solar system for hydrogen production using steam reforming of methane," International Journal of Hydrogen Energy, Available online 31 August 2024.

[16] T. -J. Huang and S. -Y. Jhao, "Ni-Cu/samaria-doped ceria catalysts for steam reforming of methane in the presence of carbon dioxide," Applied Catalysis A: General, vol. 302, no. 2, pp. 325-332, 2006.

[17] R. Kumar, A. Kumar, and A. Pal, “Simulation modelling of hydrogen production from steam reforming of methane and biogas,” Fuel, vol. 362, 130742, 2024.

[18] N. Yusuf, F. Almomani, and H. Qiblawey, “Dynamic modeling of hydrogen production from boil-off gas (BOG) at onshore LNG facilities: Technical and socio-economic analysis,” International Journal of Hydrogen Energy, vol. 67, pp. 949-958, 2024.

[19] C. Wang, D. Sun, Q. Shen, Y. Duan, and X. Huang, “A reliquefaction process of LNG boil-off gas using an improved Kapitsa cycle: Eliminating the BOG compressor,” Energy, vol. 304, 131979, 2024.

[20] L. Liu, T. Guo, Y. Zhou, J. Shen, Q. Jiang, and X. Tong, “Review of the design and optimization of BOG re-liquefaction process for LNG carriers,” Cryogenics, vol. 142, 103924, 2024.

[21] A. I. Osman, N. Mehta, A. M. Elgarahy, M. Hefny, A. Al-Hinai, *et al.*, “Hydrogen production, storage, utilisation and environmental impacts: a review,” Environmental Chemistry Letters, vol. 20, pp. 153-188, 2022.

[22] R.L. Keiski, O. Desponds, Y.-F. Chang, and G.A. Somorjai, “Kinetics of the water-gas shift reaction over several alkane activation and water-gas shift catalysts,” Applied Catalysis A: General, vol. 101, no. 2, pp. 317-338, 1993.